

000
001
002054
055
056

Multi-channel Weighted Nuclear Norm Minimization for Real Color Image Denoising

057
058
059003
004
005
006
007060
061
062
063

Anonymous ICCV submission

008
009
010
011064
065
066

Paper ID 572

012
013
014
015067
068
069

Abstract

The noise structures among the R, G, B channels of real images are quite different due to the preprocessing steps, such as demosaicing, white balance, etc., of the in-camera imaging pipelines. This makes the real image denoising problem much more complex than traditional grayscale image denoising. In this paper, we propose a multi-channel optimization model for real color image denoising. Specifically, we introduce a weighting matrix into the data term to process adaptively each part of R, G, B channels in the joint patches concatenated by corresponding patches in these channels. In the regularization term, we employ the weighted nuclear norm to exploit the non-local self similar property. The proposed multi-channel weighted nuclear norm minimization (WNNM) model is much more complex than the standard WNNM model. We reformulate the proposed model into a linear equality-constrained optimization problem and solve it by the alternating direction method of multipliers algorithm. Each alternative updating step has closed-form solution and the convergence results are given. Experiments on benchmark datasets demonstrate that the proposed model outperforms state-of-the-art denoising methods on synthetic as well as real-world noisy images.

lent denoising performance by exploiting the NSS property via low rank regularization.

The real color image denoising problem is not a trivial extension from single channel (grayscale image) to multiple channels (color image). The reason is that the noise structures are quite different among the Red (R), Green (G), Blue (B) channels of images captured by CCD or CMOS cameras due to the on-board processing steps [13]. This makes the real color image denoising problem much more complex. Directly applying the denoising methods for grayscale images to each channel of color images separately would obtain bad performance [14]. There are several work [14–19] proposed specifically for color image denoising. The method [15] first transforms the color images into the luminance/chrominance space such as YCbCr before denoising, but this would make the noise distribution more complex in color images. The methods of [14, 19] process the joint patches concatenated by the corresponding patches in R, G, B channels and treat equally the patches in different channels. This would generate false colors or artifacts [14]. The methods of [16–18] ignore the non-local self similarity property of natural images, and their performance would be largely depressed [2, 7].

In order to deal with the R, G, B channels in color images more effectively, different noise properties of different channels should be considered in solving real color image denoising problem. Besides, due to its expressive denoising performance, the WNNM model [7] is employed to exploit the NSS property of natural images. In this paper, we proposed a multi-channel WNNM model for real color image denoising. By introducing a weighting matrix to the WNNM model, the proposed multi-channel WNNM model no longer has closed-form solutions and more challenging to solve. By reformulating the proposed multi-channel WNNM model into a linear equality-constrained program with two variables, the relaxed problem can be solved under the alternating direction method of multipliers (ADMM) [20] framework. Each variable can be updated with closed-form solution [7, 21]. We also give the convergency results with detailed proof to guarantee a rational termination of

1. Introduction

Image denoising is an important problem in enhancing the image quality in computer vision systems. The traditional grayscale image denoising problem aims to recover the clean image \mathbf{x} from the noisy observation $\mathbf{y} = \mathbf{x} + \mathbf{n}$, where \mathbf{n} is often assumed to be additive white Gaussian noise (AWGN). Most image denoising methods in this field either employ the non-local self similarity (NSS) of natural images [1–7] or learn generative or discriminative denoisers from paired natural clean images and synthetic noisy images [8–12]. Among these methods, the weighted nuclear norm minimization (WNNM) method achieves exal-

108
109
110
111
112
113
114
115
116
117
118
119
120
121
122
123
124
125
126
127
128
129
130
131
132
133
134
135
136
137
138
139
140
141
142
143
144
145
146
147
148
149
150
151
152
153
154
155
156
157
158
159
160
161

the proposed algorithm.

2. Related Work

2.1. Weighted Nuclear Norm Minimization

As an extension to the nuclear norm minimization (NNM) model [22], the weighted nuclear norm minimization (WNNM) model [7] is described as

$$\min_{\mathbf{X}} \|\mathbf{Y} - \mathbf{X}\|_F^2 + \|\mathbf{X}\|_{w,*} \quad (1)$$

where $\|\mathbf{X}\|_{w,*} = \sum_i w_i \sigma_i(\mathbf{X})$ is the weighted nuclear norm of matrix \mathbf{X} , and $\mathbf{w} = [w_1, \dots, w_n]^\top$, $w_i \geq 0$ is the weight vector, $\sigma_i(\mathbf{X})$ is the i -th singular value of matrix \mathbf{X} . According to the Corollary 1 of [23], the problem (1) has closed-form solution if the weights are non-decreasing

$$\hat{\mathbf{X}} = \mathbf{U} \mathcal{S}_{w/2}(\Sigma) \mathbf{V}^\top \quad (2)$$

where $\mathbf{Y} = \mathbf{U} \Sigma \mathbf{V}^\top$ is the singular value decomposition [24] of \mathbf{Y} and $\mathcal{S}_\tau(\bullet)$ is the generalized soft-thresholding operator with weight vector \mathbf{w} :

$$\mathcal{S}_{w/2}(\Sigma_{ii}) = \max(\Sigma_{ii} - w_{ii}/2, 0) \quad (3)$$

Though having achieved excellent performance on grayscale image denoising, the WNNM model would generate false colors or artifacts [14], if being directly extended to real color image denoising by processing each channel separately or joint vectors concatenated by multiple channels. In this paper, for real noisy image denoising, we propose a multi-channel WNNM model which preserve the power of WNNM and be able to process the differences among different channels.

2.2. Real Color Image Denoising

During the last decade, several denoising methods are proposed for real color image denoising [15–17, 19]. Among them, the CBM3D [15] first transform the RGB image into luminance-chrominance space (e.g., YCbCr) and then apply the famous BM3D method [2] on each channel separately with the patches being grouped only in the luminance channel. In [16], the authors proposed the “Noise Level Function” to estimate and remove the noise for each channel in natural images. However, the methods processing each channel separately would achieve inferior performance than processing jointly these channels [14]. The methods of [17, 19, 25] perform real color image denoising by concatenating the patches in R, G, B channels into joint vectors. However, the concatenation would treat each channel equally and ignore the different noise properties among these channels. The method in [18] models the cross-channel noise in real noisy image as a multivariate Gaussian and the noise is removed by the Bayesian non-local means filter [26]. The commercial software Neat Image [27] estimates the noise parameters from a flat region of the given noisy image and filters the noise correspondingly. But these methods [18, 27] ignore the non-local self similarity property of natural images [2, 7].

In this paper, we introduce a weighting matrix which add different weights to different channels for color image denoising. The proposed multi-channel method can effectively solve the problem of different noise structures among different channels.

162
163
164
165
166
167
168
169
170
171
172
173
174
175
176
177
178
179
180
181
182
183
184
185
186
187
188
189
190
191
192
193
194
195
196
197
198
199
200
201
202
203
204
205
206
207
208
209
210
211
212
213
214
215

3. Color Image Denoising via Multi-channel Weighted Nuclear Norm Minimization

3.1. The Problem

The color image denoising problem is to recover the clean image $\{\mathbf{x}_c\}$ from its noisy version $\mathbf{y}_c = \mathbf{x}_c + \mathbf{n}_c$, where $c \in \{r, g, b\}$ is the index of R, G, B channels and \mathbf{n}_c is the noise in c -th channel. The noise structures in each channel are different due to the on-board processing of the in-camera imaging pipeline [13]. Therefore, it is problematic to directly apply denoising methods to the joint vectors concatenated by corresponding patches of the R, G, B channels. To validate this point, in Fig. 1, we show the clean image “kodim23” taken from the Kodak PhotoCD dataset, its degraded version generated by adding synthetic additive white Gaussian noise (AWGN) to each channel of “kodim23”, and the denoised image by applying WNNM [7] on the joint vectors concatenated from R, G, B channels of the degraded image. The standard derivations of AWGN added to the R, G, B channels are $\sigma_r = 40$, $\sigma_g = 20$, $\sigma_b = 30$, respectively. The input standard derivation of the noise for the concatenated WNNM method is set as the Root Mean Square (RMS) of those in each channel, i.e., $\sigma = \sqrt{(\sigma_r^2 + \sigma_g^2 + \sigma_b^2)/3} = 31.1$. From Fig. 1, one can see that the concatenated WNNM method treating each channel equally would remain some noise in the R and B channel, while oversmoothing the G channel of the degraded image. Hence, if the patches of different channels are treated adaptively in the concatenated vectors, the degraded color images would be recovered with better visual qualities.

In order to process each channel differently while still exploiting the joint structures of the color images, in this paper, we introduce a weighting matrix \mathbf{W} to the concatenated WNNM method. Assume the matrix \mathbf{Y} containing the noisy patches in R, G, B channels as $\mathbf{Y} = [\mathbf{Y}_r^\top \mathbf{Y}_g^\top \mathbf{Y}_b^\top]^\top$, the corresponding clean matrix $\mathbf{X} = [\mathbf{X}_r^\top \mathbf{X}_g^\top \mathbf{X}_b^\top]^\top$, and the weights \mathbf{w} for the singular values of \mathbf{X} , then the proposed multi-channel WNNM (MC-WNNM) model is

$$\min_{\mathbf{X}} \|\mathbf{W}(\mathbf{Y} - \mathbf{X})\|_F^2 + \|\mathbf{X}\|_{w,*..} \quad (4)$$

How to set the weighting matrix \mathbf{W} and how to solve the proposed model will be introduced in the next sections.

3.2. The Setting of Weighting Matrix \mathbf{W}

For simplicity, in this paper, we assume the noise are independent among the R, G, B channels and i.i.d. in each

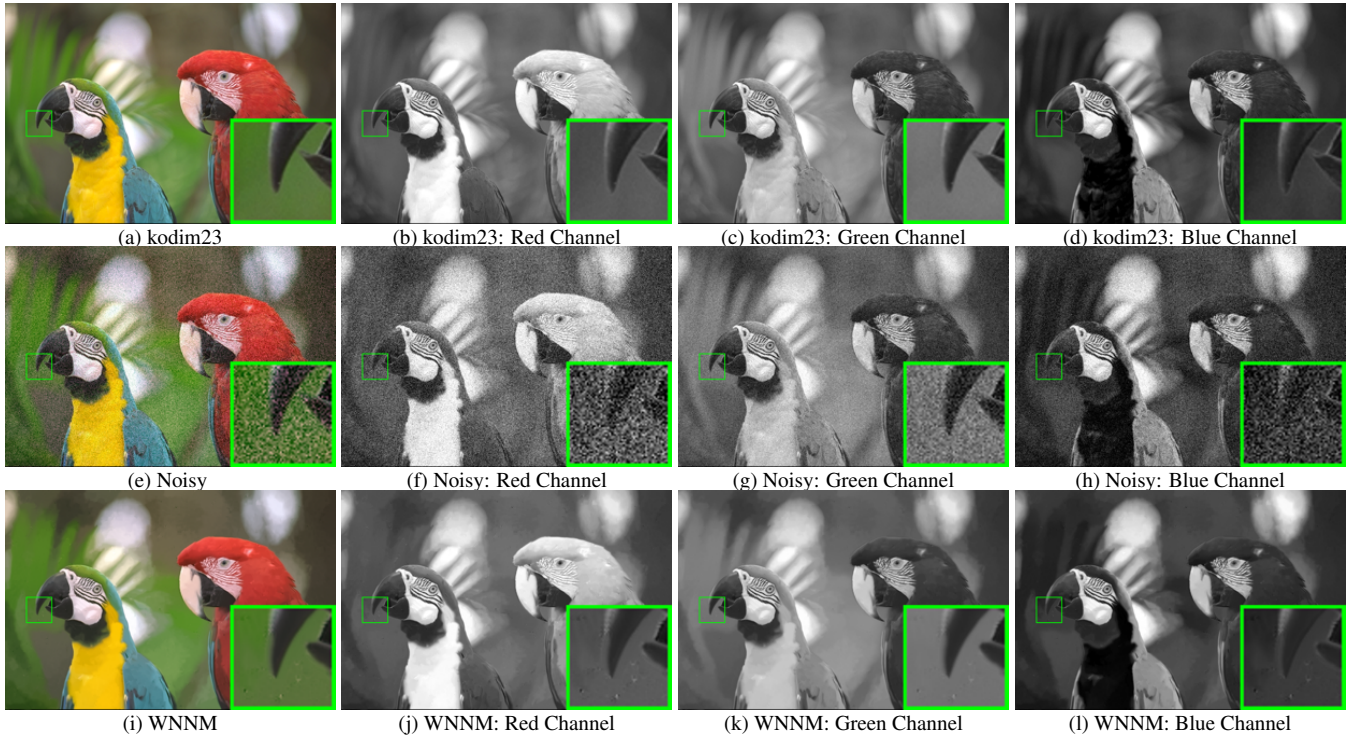


Figure 1. The image “kodim23” of the Kodak PhotoCD dataset, its degraded version, and the image recovered by WNNM. The R, G, B channels are also listed here for image quality comparison.

channel. Therefore, the weighting matrix \mathbf{W} is diagonal and can be determined under the Bayesian framework:

$$\begin{aligned} \hat{\mathbf{X}} &= \arg \max_{\mathbf{X}} \ln P(\mathbf{X}|\mathbf{Y}, \mathbf{w}) \\ &= \arg \max_{\mathbf{X}} \{ \ln P(\mathbf{Y}|\mathbf{X}) + \ln P(\mathbf{X}|\mathbf{w}) \}. \end{aligned} \quad (5)$$

The log-likelihood term $\ln P(\mathbf{Y}|\mathbf{X})$ is characterized by the statistics of noise, which is assumed to be channel-wise independent white Gaussian with standard deviations $\{\sigma_r, \sigma_g, \sigma_b\}$

$$P(\mathbf{Y}|\mathbf{X}) = \prod_{c \in \{r,g,b\}} (2\pi\sigma_c^2)^{-\frac{3p^2}{2}} \exp\left(-\frac{1}{2\sigma_c^2} \|\mathbf{Y}_c - \mathbf{X}_c\|_F^2\right). \quad (6)$$

We assume that the matrix \mathbf{X} follows the following distribution

$$P(\mathbf{X}|\mathbf{w}) \propto \exp\left(-\frac{1}{2} \|\mathbf{X}\|_{\mathbf{w},*}\right). \quad (7)$$

Putting (7) and (6) into (5), we have

$$\hat{\mathbf{X}} = \arg \min_{\mathbf{X}} \|\mathbf{W}(\mathbf{Y} - \mathbf{X})\|_F^2 + \|\mathbf{X}\|_{\mathbf{w},*}, \quad (8)$$

where

$$\mathbf{W} = \begin{pmatrix} \sigma_r^{-1} \mathbf{I} & \mathbf{0} & \mathbf{0} \\ \mathbf{0} & \sigma_g^{-1} \mathbf{I} & \mathbf{0} \\ \mathbf{0} & \mathbf{0} & \sigma_b^{-1} \mathbf{I} \end{pmatrix}. \quad (9)$$

where $\mathbf{I} \in \mathbb{R}^{p^2 \times p^2}$ is the identity matrix. Hence, the weighting matrix \mathbf{W} is determined to contribute equal weights for the pixel values in the same channel, while different weights for those in different channels. The experimental (which will be introduced later) results have already demonstrated

that this form of weighting matrix have already generated the best denoising performance on synthetic and real noisy images in benchmark datasets.

3.3. The Denoising Algorithm

In this section, with the proposed MC-WNNM model, we propose a denoising algorithm for color images. In our algorithm, given a noisy image \mathbf{y} , each local patch is extracted from it with patch size $p \times p \times 3$ and stretched to a patch vector $\mathbf{y}_j \in \mathbb{R}^{3p^2}$ concatenated by corresponding patches in R, G, B, channels. Then we search the M most similar patches to \mathbf{y}_j (including \mathbf{y}_j itself) by Euclidean distance in a $W \times W$ local region around it. We stack the M similar patches column by column to form a noisy patch matrix $\mathbf{Y}_j = \mathbf{X}_j + \mathbf{N}_j \in \mathbb{R}^{3p^2 \times M}$, where \mathbf{X}_j and \mathbf{N}_j the corresponding clean and noise patch matrices. Then, we can apply the proposed MC-WNNM model to \mathbf{Y}_j to estimate $\hat{\mathbf{X}}_j$ for color image denoising:

$$\min_{\mathbf{X}_j} \|\mathbf{W}_j(\mathbf{Y}_j - \mathbf{X}_j)\|_F^2 + \|\mathbf{X}_j\|_{\mathbf{w},*}. \quad (10)$$

where \mathbf{W}_j is defined in Eq. (9). Just as [23] did, the weight vector \mathbf{w} is set $w_i^{k+1} = \frac{C}{|\sigma_i(\mathbf{X}_k)| + \epsilon}$ and $\epsilon > 0$ is a small number to avoid zero numerator. Note that when $\sigma_r = \sigma_g = \sigma_b$, the multi-channel WNNM model will be reduced to the concatenated WNNM model as a special case.

The multi-channel WNNM is applied to the noisy patch matrix \mathbf{Y}_j of each local patch \mathbf{y}_j in the noisy image \mathbf{y} . And

324
 325 **Algorithm 1:** Color Image Denoising by MC-WNNM
 326 **Input:** Noisy image \mathbf{y} , noise levels $\{\sigma_r, \sigma_g, \sigma_b\}$;
 327 **Initialization:** $\hat{\mathbf{x}}^{(0)} = \mathbf{y}, \mathbf{y}^{(0)} = \mathbf{y}$;
 328 **for** $k = 1 : K_1$ **do**
 329 1. Set $\mathbf{y}^{(k)} = \hat{\mathbf{x}}^{(k-1)}$;
 330 2. Extracte local patches $\{\mathbf{y}_j\}_{j=1}^N$ from $\mathbf{y}^{(k)}$;
 331 **for** each patch \mathbf{y}_j **do**
 332 3. Search non-local similar patches \mathbf{Y}_j ;
 333 4. Applying the MC-WNNM model (10) to \mathbf{Y}_j and
 334 obtain the estimated \mathbf{X}_j ;
 335 **end for**
 336 5. Aggregate $\{\mathbf{X}_j\}_{j=1}^N$ to form the image $\hat{\mathbf{x}}^{(k)}$;
 337 **end for**
 338 **Output:** Denoised image $\hat{\mathbf{x}}^{K_1}$.

339 then all the patches are aggregated together to form the final
 340 recovered image $\hat{\mathbf{y}}$. To obtain better denoising results,
 341 we perform the above denoising procedure for several (K_1)
 342 iterations. The proposed MC-WNNM denoising algorithm
 343 for color images is summarized in Algorithm 1.

3.4. Optimization

344 The proposed MC-WNNM model could not be solved
 345 in an analytical form while the original WNNM model
 346 [23] could. In the WNNM model, when the weights on
 347 singular values are non-descending, the weighted nuclear
 348 norm proximal operator [23] can have global optimum with
 349 closed-form solution. However, such property is not valid
 350 for the multi-channel WNNM model. The reason is that the
 351 weighting matrix \mathbf{W} is added to the rows of matrix \mathbf{X} instead
 352 of its singular values. Besides, the elements in \mathbf{W} is
 353 not in a non-descending order with respect to the singular
 354 value of \mathbf{X} . This makes the proposed model more difficult
 355 to solve when compared to the original WNNM model.

356 By introducing an augmented variable \mathbf{Z} , the MC-
 357 WNNM model is reformulated as a linear equality-
 358 constrained problem with two variables \mathbf{X} and \mathbf{Z} :

$$359 \min_{\mathbf{X}, \mathbf{Z}} \|\mathbf{W}(\mathbf{Y} - \mathbf{X})\|_F^2 + \|\mathbf{Z}\|_{w,*} \quad \text{s.t. } \mathbf{X} = \mathbf{Z}. \quad (11)$$

360 Since the objective function is separable across the two variables,
 361 the problem (11) can be solved by under alternating direction method of multipliers (ADMM) framework. We
 362 can derive its augmented Lagrangian function:

$$363 \mathcal{L}(\mathbf{X}, \mathbf{Z}, \mathbf{A}, \rho) = \|\mathbf{W}(\mathbf{Y} - \mathbf{X})\|_F^2 + \|\mathbf{Z}\|_{w,*} \\ 364 + \langle \mathbf{A}, \mathbf{X} - \mathbf{Z} \rangle + \frac{\rho}{2} \|\mathbf{X} - \mathbf{Z}\|_F^2 \quad (12)$$

365 where \mathbf{A} is the augmented Lagrangian multiplier and $\rho > 0$
 366 is the penalty parameter. We initialize the matrix variables
 367 $\mathbf{X}_0, \mathbf{Z}_0$, and \mathbf{A}_0 to be zero matrix of suitable size. By taking
 368 derivative of the Lagrangian function \mathcal{L} with respect to the
 369 variables \mathbf{X} and \mathbf{Z} and setting the derivative function to be zero, we can alternatively update the ADMM algorithm
 370 iteratively as follows:

371 (1) **Update \mathbf{X} while fixing \mathbf{Z} and \mathbf{A} :**

$$372 \mathbf{X}_{k+1} = \arg \min_{\mathbf{X}} \|\mathbf{W}(\mathbf{Y} - \mathbf{X})\|_F^2 + \frac{\rho_k}{2} \|\mathbf{X} - \mathbf{Z}_k + \rho_k^{-1} \mathbf{A}_k\|_F^2 \quad (13)$$

373 This is a least squares regression problem with closed-form
 374 solution:

$$375 \mathbf{X}_{k+1} = (\mathbf{W}^\top \mathbf{W} + \frac{\rho_k}{2} \mathbf{I})^{-1} (\mathbf{W}^\top \mathbf{W} \mathbf{Y} + \frac{\rho_k}{2} \mathbf{Z}_k - \frac{1}{2} \mathbf{A}_k) \quad (14)$$

376 (2) **Update \mathbf{Z} while fixing \mathbf{X} and \mathbf{A} :**

$$377 \mathbf{Z}_{k+1} = \arg \min_{\mathbf{Z}} \frac{\rho_k}{2} \|\mathbf{Z} - (\mathbf{X}_{k+1} + \rho_k^{-1} \mathbf{A}_k)\|_F^2 + \|\mathbf{Z}\|_{w,*} \quad (15)$$

378 According to the Theorem 1 in [23], given the $\mathbf{X}_{k+1} + \rho_k^{-1} \mathbf{A}_k = \mathbf{U}_k \Sigma_k \mathbf{V}_k^\top$ be the SVD of $\mathbf{X}_{k+1} + \rho_k^{-1} \mathbf{A}_k$,
 379 where $\Sigma_k = \begin{pmatrix} \text{diag}(\sigma_1, \sigma_2, \dots, \sigma_n) \\ \mathbf{0} \end{pmatrix} \in \mathbb{R}^{m \times n}$, then the
 380 global optimum of the above problem is $\hat{\mathbf{Z}} = \mathbf{U}_k \hat{\Sigma}_k \mathbf{V}_k^\top$,
 381 where $\hat{\Sigma}_k = \begin{pmatrix} \text{diag}(\hat{\sigma}_1, \hat{\sigma}_2, \dots, \hat{\sigma}_n) \\ \mathbf{0} \end{pmatrix} \in \mathbb{R}^{m \times n}$ and
 382 $(\hat{\sigma}_1, \hat{\sigma}_2, \dots, \hat{\sigma}_n)$ is the solution to the following convex optimization problem:

$$383 \min_{\hat{\sigma}_1, \hat{\sigma}_2, \dots, \hat{\sigma}_n} \sum_{i=1}^n (\sigma_i - \hat{\sigma}_i)^2 + \frac{2w_i}{\rho_k} \hat{\sigma}_i \quad (16)$$

$$384 \text{s.t. } \hat{\sigma}_1 \geq \hat{\sigma}_2 \geq \dots \geq \hat{\sigma}_n \geq 0. \quad (16)$$

385 According to the Remark 1 in [23], the problem above has
 386 closed-form solution

$$387 \hat{\sigma}_i = \begin{cases} 0 & \text{if } c_2 < 0 \\ \frac{c_1 + \sqrt{c_2}}{2} & \text{if } c_2 \geq 0 \end{cases} \quad (17)$$

388 where $c_1 = \sigma_i - \epsilon$, $c_2 = (\sigma_i - \epsilon)^2 - \frac{8C}{\rho_k}$ and C is set as
 389 $\sqrt{2n}$ by experience in image denoising.

390 (3) **Update \mathbf{A} while fixing \mathbf{X} and \mathbf{Z} :**

$$391 \mathbf{A}_{k+1} = \mathbf{A}_k + \rho_k (\mathbf{X}_{k+1} - \mathbf{Z}_{k+1}) \quad (18)$$

392 (4) **Update ρ_k :** $\rho_{k+1} = \mu * \rho_k$, where $\mu > 1$.

393 The above alternative updating steps are repeated until the convergence condition is satisfied or the number of iterations exceeds a preset maximum number, e.g., K_2 . The convergence condition of the ADMM algorithm is: $\|\mathbf{X}_{k+1} - \mathbf{Z}_{k+1}\|_F \leq \text{Tol}$, $\|\mathbf{X}_{k+1} - \mathbf{X}_k\|_F \leq \text{Tol}$, and $\|\mathbf{Z}_{k+1} - \mathbf{Z}_k\|_F \leq \text{Tol}$ are simultaneously satisfied, where $\text{Tol} > 0$ is a small tolerance. We summarize the optimization steps in Algorithm 2. The convergence analysis of the proposed Algorithm 2 is given in Theorem 1. Note that since the weighted nuclear norm is non-convex in general, we employ an unbounded sequence of $\{\rho_k\}$ here to make sure that the Algorithm 2 is convergent.

394 **Theorem 1.** Assume the weights in w are in a non-
 395 descending order, the sequence $\{\mathbf{X}_k\}$, $\{\mathbf{Z}_k\}$, and $\{\mathbf{A}_k\}$
 396 generated in Algorithm 1 satisfy:

$$397 (a) \lim_{k \rightarrow \infty} \|\mathbf{X}_{k+1} - \mathbf{Z}_{k+1}\|_F = 0; \quad (19)$$

$$398 (b) \lim_{k \rightarrow \infty} \|\mathbf{X}_{k+1} - \mathbf{X}_k\|_F = 0; \quad (20)$$

$$399 (c) \lim_{k \rightarrow \infty} \|\mathbf{Z}_{k+1} - \mathbf{Z}_k\|_F = 0. \quad (21)$$

Algorithm 2: Solve MC-WNNM via ADMM

Input: Matrices \mathbf{Y} and \mathbf{W} , $\mu > 1$, $\text{Tol} > 0$;

Initialization: $\mathbf{X}_0 = \mathbf{Z}_0 = \mathbf{A}_0 = \mathbf{0}$, $\rho_0 > 0$, $\text{T} = \text{False}$, $k = 0$;

While ($\text{T} == \text{false}$) **do**

1. Update \mathbf{X}_{k+1} as

$$\mathbf{X}_{k+1} = (\mathbf{W}^\top \mathbf{W} + \frac{\rho_k}{2} \mathbf{I})^{-1} (\mathbf{W}^\top \mathbf{W} \mathbf{Y} + \frac{\rho_k}{2} \mathbf{Z}_k - \frac{1}{2} \mathbf{A}_k)$$
2. Update \mathbf{Z}_{k+1} by solving the problem

$$\min_{\mathbf{Z}} \frac{\rho_k}{2} \|\mathbf{Z}\|_F^2 + \|\mathbf{Z}\|_{w,*}$$
3. Update \mathbf{A}_{k+1} as $\mathbf{A}_{k+1} = \mathbf{A}_k + \rho_k (\mathbf{X}_{k+1} - \mathbf{Z}_{k+1})$
4. Update $\rho_{k+1} = \mu * \rho_k$;
5. $k \leftarrow k + 1$;
if (Convergence conditions are satisfied) or ($k \geq K_2$)
5. $\text{T} \leftarrow \text{True}$
end if

end while

Output: Matrices \mathbf{X} and \mathbf{Z} .

Proof. We give proof sketch here and detailed proof of this theorem can be found in supplementary files. We can first proof that the sequence $\{\mathbf{A}_k\}$ generated by Algorithm 3.4 is upper bounded. Since $\{\rho_k\}$ is unbounded, that is $\lim_{k \rightarrow \infty} \rho_k = +\infty$, we can proof that the sequence of Lagrangian function $\{\mathcal{L}(\mathbf{X}_{k+1}, \mathbf{Z}_{k+1}, \mathbf{A}_k, \rho_k)\}$ is also upper bounded. Hence, both $\{\mathbf{W}(\mathbf{Y} - \mathbf{X}_k)\}$ and $\{\mathbf{Z}_k\}$ are upper bounded. According to Eq. (18), we can proof that $\lim_{k \rightarrow \infty} \|\mathbf{X}_{k+1} - \mathbf{Z}_{k+1}\|_F = \lim_{k \rightarrow \infty} \rho_k^{-1} \|\mathbf{A}_{k+1} - \mathbf{A}_k\|_F = 0$, and (a) is proofed. Then we can proof that $\lim_{k \rightarrow \infty} \|\mathbf{X}_{k+1} - \mathbf{X}_k\|_F \leq \lim_{k \rightarrow \infty} \|(\mathbf{W}^\top \mathbf{W} + \frac{\rho_k}{2} \mathbf{I})^{-1} (\mathbf{W}^\top \mathbf{W} \mathbf{Y} - \mathbf{W}^\top \mathbf{W} \mathbf{Z}_k - \frac{1}{2} \mathbf{A}_k)\|_F + \rho_k^{-1} \|\mathbf{A}_k - \mathbf{A}_{k-1}\|_F = 0$ and hence (b) is proofed. Then (c) can be proofed by checking that $\lim_{k \rightarrow \infty} \|\mathbf{Z}_{k+1} - \mathbf{Z}_k\| \leq \lim_{k \rightarrow \infty} \|\Sigma_{k-1} - \mathcal{S}_{w/\rho_{k-1}}(\Sigma_{k-1})\|_F + \|\mathbf{X}_{k+1} - \mathbf{X}_k\|_F + \rho_k^{-1} \|\mathbf{A}_{k-1} + \mathbf{A}_{k+1} - \mathbf{A}_k\|_F = 0$, where $\mathbf{U}_{k-1} \Sigma_{k-1} \mathbf{V}_{k-1}^\top$ is the SVD of the matrix $\mathbf{X}_k + \rho_{k-1} \mathbf{A}_{k-1}$. \square

4. Experiments

We evaluate the proposed MC-WNNM method on synthetic and real color image denoising. We compare the proposed method with other state-of-the-art denoising methods including CBM3D [15], MLP [10], WNNM [7], TNRD [12], “Noise Clinic” (NC) [17, 25], and the commercial software Neat Image (NI) [27].

4.1. Implementation Details

In synthetic experiments, the noise levels in R, G, B channels are assumed to be known as $\sigma_r, \sigma_g, \sigma_b$. In the real cases, the noise levels in R, G, B channels can be estimated via noise estimation methods [28, 29]. In this paper, we employ the method of [29] for its state-of-the-art performance. For the CBM3D method [15], the input noise levels are the Root Mean Square (RMS) as

$$\sigma = \sqrt{(\sigma_r^2 + \sigma_g^2 + \sigma_b^2)/3}. \quad (22)$$

For the methods of MLP [10] and TNRD [12], we retrain the models on grayscale images following their corresponding strategies at different noise levels from $\sigma = 5$ to $\sigma = 75$ with gap of 5. The denoising on color images is performed by processing separately each channel with the model trained at the same (or nearest) noise levels. NC [17, 25] is a blind image denoising method, so we just submit the noisy images (synthetic or real) to [25] and perform denoising using the default parameters. NI [27] is a commercial software suitable for real image denoising, while the code of CC [18] is not released (but its results on the 15 real noisy images in [18] are available by requesting the authors). Hence, we only compare with CC and NI in real image denoising experiments, and do not compare with them in synthetic experiments.

In order to take fully comparison with the original WNNM method [23], we extended the WNNM method [23] for color image denoising in three directions: 1) we apply the WNNM method [23] on each channel separately with corresponding noise levels $\sigma_r, \sigma_g, \sigma_b$. We call this method “WNNM0”; 2) we perform denoising on the joint vectors concatenated by corresponding patches in the R, G, B channels, where the input noise level σ is computed by RMS (Eq. (22)). We call this method “WNNM1”; 3) we set the weighting matrix \mathbf{W} in the proposed MC-WNNM model as $\mathbf{W} = \sigma^{-1} \mathbf{I}$. For fair comparison, we tune all these methods set the same parameters for “WNNM2” and the proposed MC-WNNM methods while achieving the best performance of “WNNM2”. For fair comparison, we tune the methods of “WNNM0”, “WNNM1”, “WNNM2”, and the proposed MC-WNNM to achieve corresponding best denoising performance (i.e., highest average PSNR results).

4.2. Experiments on Synthetic Noisy Images

In this section, we compare the proposed MC-WNNM method with other competing method [10, 12, 15, 17, 27] as well as the three extensions of WNNM [23] on the 24 high quality color images from the Kodak PhotoCD Dataset (<http://r0k.us/graphics/kodak/>), which are shown in Fig. 2. The noisy images are generated by adding additive white Gaussian noise (AWGN) with known standard derivations $\sigma_r, \sigma_g, \sigma_b$ for the R, G, B channels, respectively. In this paper, the noise levels we add to each channel of the 24 color images are $\sigma_r = 40, \sigma_g = 20, \sigma_b = 30$, respectively. More experiments can be found in the supplementary files. For the methods of “WNNM2” and MC-WNNM, we set the patch size as $p = 6$, the number of non-local similar patches as $M = 70$, the window size for searching similar patches as $W = 20$, the updating parameter $\mu = 1.001$, the number of iterations in Algorithm 1 as $K_1 = 8$, the number of iterations in Algorithm 2 as $K_2 = 10$. For “WNNM2”, the initial penalty parameter is set as $\rho_0 = 10$, while for the



540
541
542
543
544
545
546
547
548
549
550
551
552
553
554
555
556
557
558
559
560
561
562
563
564
565
566
567
568
569
570
571
572
573
574
575
576
577
578
579
580
581
582
583
584
585
586
587
588
589
590
591
592
593
Figure 2. The 24 high quality color images from the Kodak PhotoCD Dataset.

proposed MC-WNNM model, the penalty parameter is set as $\rho_0 = 3$.

The PSNR results are listed in Table 1 of the compared methods including CBM3D [15], MLP [10], TNRD [12], NC [17, 25], “WNNM0” [23], “WNNM1”, “WNNM2” and the proposed MC-WNNM methods. The best PSNR results are highlighted in bold. One can see that on all the 24 images, our method achieves the highest PSNR values over the competing methods. On average PSNR, our proposed method achieves 0.48dB improvements over the “WNNM0” method and outperforms the “WNNM2” by 1.09dB. Fig. 3 shows a scene denoised by the compared methods. We can see that CBM3D and NC would remain noise while MLP and TNRD would generate artifacts. The methods of “WNNM0”, “WNNM1”, “WNNM2” would over-smooth much the image. By using the proposed MC-WNNM model, our method preserves the structures (e.g., edges and textures) better across the R, G, B channels and generate less artifacts than other denoising methods, leading to visually pleasant outputs. More visual comparisons can be found in the supplementary files.

4.3. Experiments on Real Noisy Images

In this section, we compare the proposed MC-WNNM method with other competing methods on the 15 real noisy images (Fig. 4). We do not compare with the “WNNM0” method due to limited space and its inferior performance. The noisy images were collected under controlled indoor environment. Each scene was shot 500 times under the same camera and camera setting. The mean image of the 500 shots is roughly taken as the “ground truth”, with which the PSNR can be computed. Since the image size is very large (about 7000×5000) and the 11 scenes share repetitive contents, the authors of [18] cropped 15 smaller images (of size 512×512) to perform experiments. For each real noisy image, the noise levels in R, G, B channels are estimated by [29]. Since the noise levels are small in real noisy images, for the method of MLP [10] and TNRD [12], we apply the trained models of corresponding methods and choose the best denoising results (highest average PSNR values). Both methods achieves best results when setting the noise levels

of the trained models from $\sigma = 10$.

We perform quantitative comparison on the 15 cropped images used in [18]. The PSNR results are listed in Table 2 of the compared methods including CBM3D [15], MLP [10], TNRD [12], NC [17, 25], NI [27], CC [18] (copied from [18]), “WNNM1”, “WNNM2”, and the proposed MC-WNNM method. The highest PSNR results are highlighted in bold. On average PSNR, the proposed MC-WNNM method achieves 0.44dB improvements over the “WNNM1” method and outperforms the state-of-the-art denoising method CC [18] by 0.83dB. On 10 out of the whole 15 images, the proposed MC-WNNM method achieves the highest PSNR values. Both CC and “WNNM1” achieves highest PSNR results on 2 of 15 images. It should be noted that in the CC method, a specific model is trained for each camera and camera setting, while our method uses the same model for all images. Fig. 5 shows the denoised images of a scene captured by Canon 5D Mark 3 at ISO = 3200. We can see that CBM3D, NC, NI and CC would either remain noise or generate artifacts, while MLP, TNRD over-smooth much the image. By using the proposed MC-WNNM model achieves better visual quality results than other methods. More visual comparisons can be found in the supplementary files.

5. Conclusion and Future Work

Most existing color image denoising methods treat the R, G, B channels equally and ignore the different noise structures in different channels. Common strategies that processing each channel separately and concatenating the RGB values into joint vectors would generate false color or artifacts. In this paper, we proposed a noval model for color image denoising which can explore the different noise structures among the R, G, B channels and exploit the non-local self similarity property of natural images. Specifically, we introduced a weighting matrix, which are employed to describe the noise levels of different channels, to the original weighted nuclear norm minimization (WNNM) model. Though the proposed model no longer has closed-form solution, we successfully solved the proposed model via the famous ADMM algorithm by introducing an additional variable with a linear constraint. The transformed problem has convergence property and can be solved in an alternative updating manner and both variables can be updated with closed-form solutions. We applied the proposed multi-channel WNNM model on color image denoising problem. Extensive experiments on benchmark datasets demonstrate that the proposed model outperforms the other competing denoising methods on both synthetic color noisy images as well as real-world noisy images. The introduce of the weighting matrix can indeed boost the performance of the original WNNM model on color image denoising. We believe that this work can be extended in at least three direc-

594
595
596
597
598
599
600
601
602
603
604
605
606
607
608
609
610
611
612
613
614
615
616
617
618
619
620
621
622
623
624
625
626
627
628
629
630
631
632
633
634
635
636
637
638
639
640
641
642
643
644
645
646
647

648
649
650
651
652
653
654
655
656
657
658
659
660
661
662
663
664
665
666
667
668
669
670
671
672
673
674
675
676
677
678
679
680
681
682
683
684
685
686
687
688
689
690
691
692
693
694
695
696
697
698
699
700
701

Table 1. PSNR(dB) results of different denoising algorithms on 24 natural images.

Image#	$\sigma_r = 40, \sigma_g = 20, \sigma_b = 30$								
	CBM3D	MLP	TNRD	NI	NC	WNNM0	WNNM1	WNNM2	MC-WNNM
1	25.24	25.70	25.74	23.85	24.90	26.01	25.95	25.58	26.66
2	28.27	30.12	30.21	25.90	25.87	30.08	30.11	29.80	30.20
3	28.81	31.19	31.49	26.00	28.58	31.58	31.61	31.20	32.25
4	27.95	29.88	29.86	25.82	25.67	30.13	30.16	29.84	30.49
5	25.03	26.00	26.18	24.38	25.15	26.44	26.39	25.32	26.82
6	26.24	26.84	26.90	24.65	24.74	27.39	27.30	26.88	27.98
7	27.88	30.28	30.40	25.63	27.69	30.47	30.54	29.70	30.98
8	25.05	25.59	25.83	24.02	25.30	26.71	26.75	25.26	26.90
9	28.44	30.75	30.81	25.94	27.44	30.86	30.92	30.29	31.49
10	28.27	30.38	30.57	25.87	28.42	30.65	30.68	29.95	31.26
11	26.95	28.00	28.14	25.32	24.67	28.19	28.16	27.61	28.63
12	28.76	30.87	31.05	26.01	28.37	30.97	31.06	30.58	31.48
13	23.76	23.95	23.99	23.53	22.76	24.27	24.15	23.52	24.89
14	26.02	26.97	27.11	24.94	25.68	27.20	27.15	26.55	27.57
15	28.38	30.15	30.44	26.06	28.21	30.52	30.60	30.13	30.81
16	27.75	28.82	28.87	25.69	26.66	29.27	29.21	29.02	29.96
17	27.90	29.57	29.80	25.85	28.32	29.78	29.79	29.16	30.40
18	25.77	26.40	26.41	24.74	25.70	26.63	26.56	26.01	27.22
19	27.30	28.67	28.81	25.40	26.52	29.19	29.22	28.67	29.57
20	28.96	30.40	30.76	24.95	25.90	30.79	30.83	29.97	31.07
21	26.54	27.53	27.60	25.06	26.48	27.80	27.75	27.12	28.34
22	27.05	28.17	28.27	25.36	26.60	28.21	28.16	27.81	28.64
23	29.14	32.31	32.51	26.13	23.24	31.89	31.97	31.21	32.34
24	25.75	26.41	26.53	24.55	25.73	27.10	27.03	26.18	27.59
Average	27.13	28.54	28.68	25.24	26.19	28.84	28.83	28.22	29.31

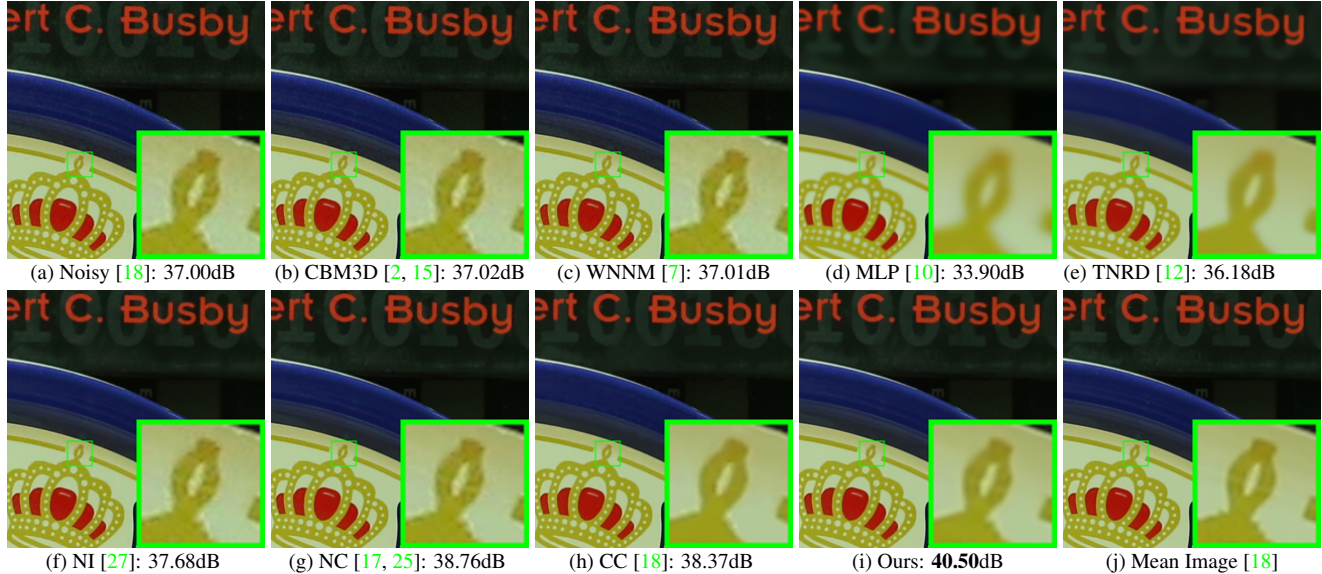


Figure 3. Denoised images of a region cropped from the real noisy image “Canon 5D Mark 3 ISO 3200 1” [18] by different methods. The images are better to be zoomed in on screen.

tions. Firstly, the proposed weighting matrix can be introduced into other methods designed for denoising grayscale images. Secondly, the weighting matrix beyond the diagonal form, such as correlation form [30], may bring better performance on color image denoising. Thirdly, the proposed multi-channel WNNM model can be further extended to deal with images with more channels, such as the hyperspectral images in remote sensing applications. We will focus our future work on these three directions.

References

- [1] A. Buades, B. Coll, and J. M. Morel. A non-local algorithm for image denoising. *IEEE Conference on Computer Vision and Pattern Recognition (CVPR)*, pages 60–65, 2005. **1**
- [2] K. Dabov, A. Foi, V. Katkovnik, and K. Egiazarian. Image denoising by sparse 3-D transform-domain collaborative filtering. *IEEE Transactions on Image Processing*, 16(8):2080–2095, 2007. **1, 2, 7, 9**
- [3] M. Elad and M. Aharon. Image denoising via sparse

Table 2. PSNR(dB) results of different methods on 15 cropped real noisy images used in [18].

Camera Settings	CBM3D	MLP	TNRD	NI	NC	CC	WNNM1	WNNM2	MC-WNNM
Canon 5D Mark III ISO = 3200	39.76	39.00	39.51	35.68	36.20	38.37	39.74	39.98	41.13
	36.40	36.34	36.47	34.03	34.35	35.37	35.12	36.65	37.28
	36.37	36.33	36.45	32.63	33.10	34.91	33.14	34.63	36.52
Nikon D600 ISO = 3200	34.18	34.70	34.79	31.78	32.28	34.98	35.08	35.08	35.53
	35.07	36.20	36.37	35.16	35.34	35.95	36.42	36.84	37.02
	37.13	39.33	39.49	39.98	40.51	41.15	40.78	39.24	39.56
Nikon D800 ISO = 1600	36.81	37.95	38.11	34.84	35.09	37.99	38.28	38.61	39.26
	37.76	40.23	40.52	38.42	38.65	40.36	41.24	40.81	41.43
	37.51	37.94	38.17	35.79	35.85	38.30	38.04	38.96	39.55
Nikon D800 ISO = 3200	35.05	37.55	37.69	38.36	38.56	39.01	39.93	37.97	38.91
	34.07	35.91	35.90	35.53	35.76	36.75	37.32	37.30	37.41
	34.42	38.15	38.21	40.05	40.59	39.06	41.52	38.68	39.39
Nikon D800 ISO = 6400	31.13	32.69	32.81	34.08	34.25	34.61	35.20	34.57	34.80
	31.22	32.33	32.33	32.13	32.38	33.21	33.61	33.43	33.95
	30.97	32.29	32.29	31.52	31.76	33.22	33.62	34.02	33.94
Average	35.19	36.46	36.61	35.33	35.65	36.88	37.27	37.12	37.71



Figure 4. The 15 cropped real noisy images used in [18].

and redundant representations over learned dictionaries. *IEEE Transactions on Image Processing*, 15(12):3736–3745, 2006.

- [4] J. Mairal, F. Bach, J. Ponce, G. Sapiro, and A. Zisserman. Non-local sparse models for image restoration. *IEEE International Conference on Computer Vision (ICCV)*, pages 2272–2279, 2009.
- [5] W. Dong, L. Zhang, G. Shi, and X. Li. Nonlocally centralized sparse representation for image restoration. *IEEE Transactions on Image Processing*, 22(4):1620–1630, 2013.
- [6] J. Xu, L. Zhang, W. Zuo, D. Zhang, and X. Feng. Patch group based nonlocal self-similarity prior learning for image denoising. *IEEE International Conference on Computer Vision (ICCV)*, pages 244–252, 2015.
- [7] S. Gu, L. Zhang, W. Zuo, and X. Feng. Weighted nuclear norm minimization with application to image denoising. *IEEE Conference on Computer Vision and Pattern Recognition (CVPR)*, pages 2862–2869, 2014. 1, 2, 5, 7, 9

Recognition (CVPR), pages 2862–2869, 2014. 1, 2, 5, 7, 9

- [8] S. Roth and M. J. Black. Fields of experts. *International Journal of Computer Vision*, 82(2):205–229, 2009. 1
- [9] D. Zoran and Y. Weiss. From learning models of natural image patches to whole image restoration. *IEEE International Conference on Computer Vision (ICCV)*, pages 479–486, 2011.
- [10] H. C. Burger, C. J. Schuler, and S. Harmeling. Image denoising: Can plain neural networks compete with BM3D? *IEEE Conference on Computer Vision and Pattern Recognition (CVPR)*, pages 2392–2399, 2012. 5, 6, 7, 9
- [11] U. Schmidt and S. Roth. Shrinkage fields for effective image restoration. *IEEE Conference on Computer Vision and Pattern Recognition (CVPR)*, pages 2774–2781, June 2014.
- [12] Y. Chen, W. Yu, and T. Pock. On learning optimized reaction diffusion processes for effective image restoration. *IEEE Conference on Computer Vision and Pattern Recognition (CVPR)*, pages 5261–5269, 2015. 1, 5, 6, 7, 9
- [13] H. C. Karaimer and M. S. Brown. A software platform for manipulating the camera imaging pipeline. *European Conference on Computer Vision (ECCV)*, October 2016. 1, 2
- [14] Julien Mairal, Michael Elad, and Guillermo Sapiro. Sparse representation for color image restoration. *IEEE Transactions on Image Processing*, 17(1):53–69, 2008. 1, 2
- [15] K. Dabov, A. Foi, V. Katkovnik, and K. Egiazarian. Color image denoising via sparse 3D collaborative filtering with grouping constraint in luminance-chrominance space. *IEEE International Conference on Image Processing (ICIP)*, pages 313–316, 2007. 1, 2, 5, 6, 7, 9

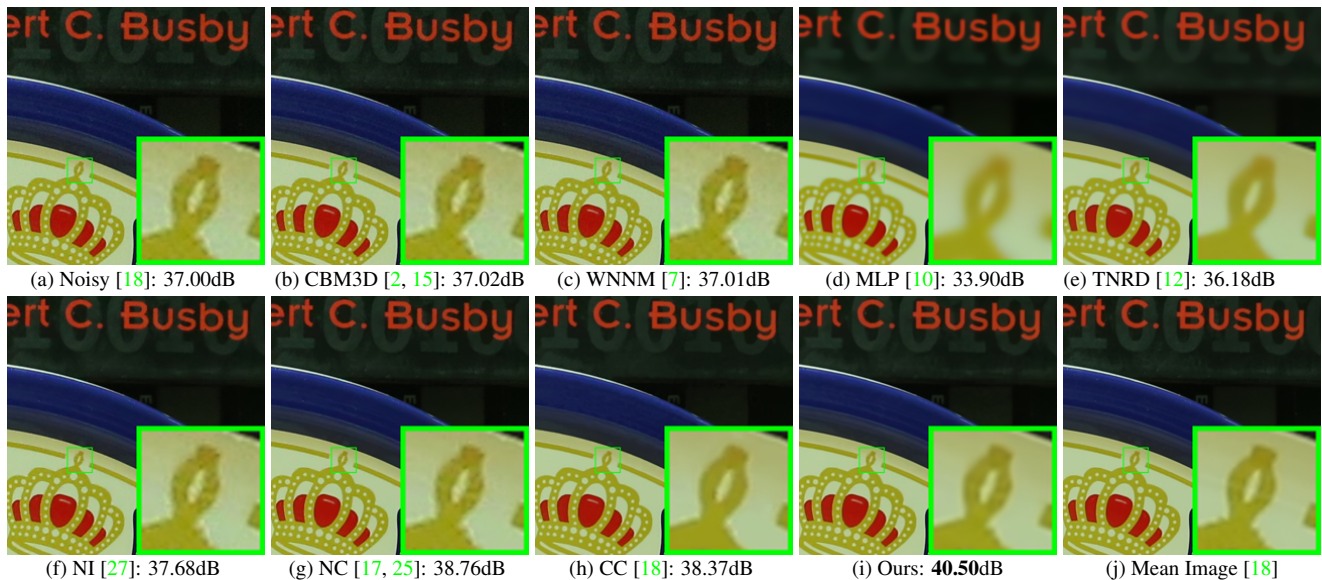


Figure 5. Denoised images of a region cropped from the real noisy image “Canon 5D Mark 3 ISO 3200 1” [18] by different methods. The images are better to be zoomed in on screen.

- [16] C. Liu, R. Szeliski, S. Bing Kang, C. L. Zitnick, and W. T. Freeman. Automatic estimation and removal of noise from a single image. *IEEE Transactions on Pattern Analysis and Machine Intelligence*, 30(2):299–314, 2008. 1, 2
- [17] M. Lebrun, M. Colom, and J.-M. Morel. Multiscale image blind denoising. *IEEE Transactions on Image Processing*, 24(10):3149–3161, 2015. 2, 5, 6, 7, 9
- [18] S. Nam, Y. Hwang, Y. Matsushita, and S. J. Kim. A holistic approach to cross-channel image noise modeling and its application to image denoising. *IEEE Conference on Computer Vision and Pattern Recognition (CVPR)*, pages 1683–1691, 2016. 1, 2, 5, 6, 7, 8, 9
- [19] F. Zhu, G. Chen, and P.-A. Heng. From noise modeling to blind image denoising. *IEEE Conference on Computer Vision and Pattern Recognition (CVPR)*, June 2016. 1, 2
- [20] S. Boyd, N. Parikh, E. Chu, B. Peleato, and J. Eckstein. Distributed optimization and statistical learning via the alternating direction method of multipliers. *Found. Trends Mach. Learn.*, 3(1):1–122, January 2011. 1
- [21] C. Lu, C. Zhu, C. Xu, S. Yan, and Z. Lin. Generalized singular value thresholding. *AAAI*, 2015. 1
- [22] J. Cai, E. J. Candès, and Z. Shen. A singular value thresholding algorithm for matrix completion. *SIAM Journal on Optimization*, 20(4):1956–1982, 2010. 2
- [23] S. Gu, Q. Xie, D. Meng, W. Zuo, X. Feng, and L. Zhang. Weighted nuclear norm minimization and its applications to low level vision. *International Journal of Computer Vision*, pages 1–26, 2016. 2, 3, 4, 5, 6

[24] C. Eckart and G. Young. The approximation of one matrix by another of lower rank. *Psychometrika*, 1(3):211–218, 1936. 2

[25] M. Lebrun, M. Colom, and J. M. Morel. The noise clinic: a blind image denoising algorithm. <http://www.ipol.im/pub/art/2015/125/>. Accessed 01 28, 2015. 2, 5, 6, 7, 9

[26] C. Kervrann, J. Boulanger, and P. Coupé. Bayesian non-local means filter, image redundancy and adaptive dictionaries for noise removal. *International Conference on Scale Space and Variational Methods in Computer Vision*, pages 520–532, 2007. 2

[27] Neatlab ABSoft. Neat Image. <https://ni.neatvideo.com/home>. 2, 5, 6, 7, 9

[28] X. Liu, M. Tanaka, and M. Okutomi. Single-image noise level estimation for blind denoising. *IEEE Transactions on Image Processing*, 22(12):5226–5237, 2013. 5

[29] G. Chen, F. Zhu, and A. H. Pheng. An efficient statistical method for image noise level estimation. *IEEE International Conference on Computer Vision (ICCV)*, December 2015. 5, 6

[30] N. J. Higham. Computing the nearest correlation matrix problem from finance. *IMA Journal of Numerical Analysis*, 22(3):329, 2002. 7

918
919
920
921
922
923
924
925
926
927
928
929
930
931
932
933
934
935
936
937
938
939
940
941
942
943
944
945
946
947
948
949
950
951
952
953
954
955
956
957
958
959
960
961
962
963
964
965
966
967
968
969
970
971